Check for updates

Synthesis and characterization of Ca doped ZnO thin films by sol–gel method

Anca-Ionela Istrate [1] · Florin Nastase[1] · Iuliana Mihalache[1] · Florin Comanescu[1] · Raluca Gavrila[1] · Oana Tutunaru[1] · Cosmin Romanitan[1,2] · Vasilica Tucureanu[1,3] · Monica Nedelcu[4] · Raluca Müller[1]

Abstract

ZnO thin films were synthesized using sol–gel method at 0.25 and 0.5 M molarity concentration. Moreover, the obtained thin films were Calcium-doped with 1 and 5 at% concentration. In order to investigate the structural changes in the molecular binding between ZnO and Ca, Fourier Transform Infrared spectroscopy (FTIR), Micro-Raman Spectroscopy and X-ray diffraction (XRD) were performed. The surface morphology and the chemical constituents distribution of the films were studied through Scanning Electron Microscopy (SEM), energy-dispersive X-ray spectroscopy (EDX) and Atomic Force Microscopy (AFM), respectively. The optical and electrical properties were studied by UV–Vis spectroscopy, Spectral ellipsometry and electrical I–V measurements. The results show that the properties of prepared ZnO thin films were strongly influenced by the molarity concentration and Ca-dopant. The band shape obtained at FTIR is a band attributable to metal oxide bonds and can be attributed to the vibrational assignment of Zn–O bond. SEM-EDX and AFM investigations reveal an enlarged surface area due to the porous nature of the thin films and confirm the presence of Ca in the ZnO matrix. The XRD and Raman analyses indicate the achievement of the high crystalline quality and confirm the wurtzite phase of the synthesized thin films. The films transmittance spectra indicate values between 81 and 93% in the 350–800 nm wavelength region. We further performed I–V characteristics, resulting that Ca has a different impact of the electrical performances.

Graphical Abstract
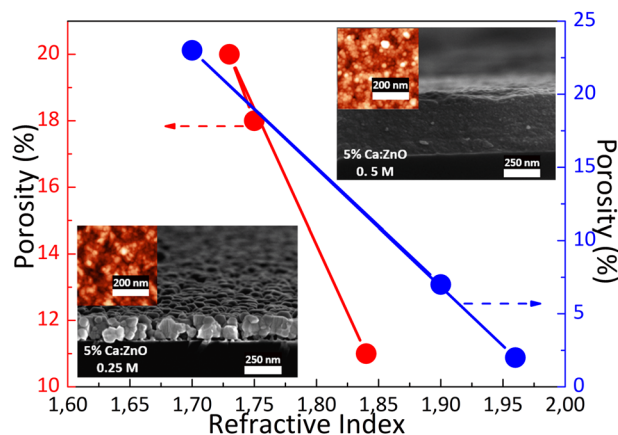
✉ Anca-Ionela Istrate
anca.istrate@imt.ro

1 National Institute for Research and Development in Microtechnologies—IMT Bucharest, 126A Erou Iancu Nicolae Street, Bucharest 077190, Romania

2 Faculty of Physics, University of Bucharest, 405 Atomistilor Street, Magurele 077125, Romania

3 Department of Materials Science, Transilvania University of Brasov, 29 Eroilor Street, Brasov 500036, Romania

4 S.C. Romquartz S.A., 126A Erou Iancu Nicolae Street, Bucharest 077190, Romania

Highlights

- Effect of Ca doping on morphological, structural, and opto-electrical properties of ZnO thin films synthesized by sol–gel at 0.25 and 0.5 M is studied.
- The films has a porous nature and a strong preferred orientation of (002) reflex when the concentration of Ca is greater.
- EDX study reveals the substitution of Ca atoms into ZnO lattice.
- Ca-doped ZnO thin films at 0.5 M exhibit superior properties when compared with 0.25 M.
- The 5 at%-Ca:ZnO, 0.5 M present the lowest resistivity value of 4.70 Ω cm.

Keywords   ZnO films · Sol–gel method · Surface morphology · Structural analysis · Electrical and optical properties

1 Introduction

In the past decade, many studies have been conducted to enhanced gas sensing of zinc oxide (ZnO) thin films through doping with different metal elements in order to improve their structural and electrical properties [1]. Recently, calcium doped zinc oxide (Ca:ZnO) thin films received attention due to their remarkable properties, such as high chemical stability, large electromechanical coupling coefficient, high piezoelectric coefficient, and low acoustic absorption, which are used in thin-film transistors [2, 3], micro-electromechanical systems [4, 5], and surface acoustic wave (SAW) [6, 7] devices. Furthermore, Ca:ZnO thin films are widely used as sensing metal oxide materials for the detection of gases like CO_2, CO, and NO_2. Thus, doping is a successful strategy to increase the selectivity toward the target gas by enhancing gas adsorption, promoting specific reactions via catalytic or electronic effects or modifying the surface [8]. Also, by controlling the Ca concentrations one can obtain a suitable ZnO guiding layer for Love wave sensor applications. Moreover, at the same thickness, a sensor with rough and porous guiding layer has a higher sensitivity compared with a smooth and dense guiding layer [9]. Recently, Dhahri et al. [10] demonstrated that sensitivity is highly increased in the presence of 5 at% Ca:ZnO prepared by sol–gel method using supercritical drying in ethyl alcohol. This study agrees with Hjiri et al. [11] that 5 at% Ca:ZnO nanoparticles present a high sensitivity and a good selectivity to CO_2 gas due to the fact that Ca creates basic centers on the surface of the material. There is a strong interaction between these basic centers and the acid CO_2 gas molecules, which leads to the formation of carbonates and bicarbonates species. Also, this result was confirmed by Dhahri et al. [12] who studied an optimized sensor, based on ZnO co-doped with 3 at% Ca and 1 at% Al that showed promising performance towards CO_2 measurement, ensuring high response and fast dynamics at operating temperature as low as 200 °C. Also, Mahdhi et al. [13] reported polycrystalline and transparent Ca:ZnO thin films with a visible transmittance higher than 80% and a minimum resistivity of 5×10^{-3} Ω cm for 3 at% Ca:ZnO

deposited by magnetron sputtering using nanocrystalline particles previously elaborated by sol–gel method.

Presently, there are scarce studies about the calcium doped ZnO thin films deposited on solid substrates like glass and Si/SiO$_2$ with the use of powder coating, supercritical drying in ethyl alcohol or sol–gel spin-coating method. Sol–gel technique involves the transformation of a molecular precursor onto a stable condensed oxide network during several stages, including hydrolysis and polymerization for the formation of the sol precursor fallowed by condensation, dehydration, nucleation, and growth, which is commonly achieved through annealing [14]. Moreover, the advantage of this method is that one can obtain high surface morphology at lower crystallizing temperature, which implies low costs [15]. In this paper, we focused on the sol–gel spin-coating preparation method of the ZnO thin films, also, considering that throughout sol–gel the porosity can be tuned resulting in a significant tailoring of the bandgap energy and the refractive index of thin films, which could improve the sensitivity and response time of ZnO based sensors [16]. Doping the ZnO nanostructured oxide films with elements of group II, such as, Be, Mg, Ca, Sr, Ba leads to the modification of the grain size at the nanoscale and, therefore, the selectivity and sensitivity of the structure. However, the synthesis of $Zn_{1-x}Ca_xO$ alloy have been focused mainly on RF-sputtering [17], pulsed laser deposition [18], and electro-spinning [19] in the form of nanoparticles [20] and nanostructures [21].

In this work, we prepared high quality Ca doped ZnO thin films by the sol–gel method with a careful selection of the precursors systems and molarity of the solutions and their structural, electrical, and optical properties have been investigated. We succesfully incorporated Ca in ZnO lattice and modified surface morphology (e.g., surface porosity, grain size, and roughness), structural parameters (e.g., lattice constants, mean crystal size, lattice strain), and optical properties (e.g., volume porosity, refractive index, band gap value, and transmitance). It is clear that the obtained films are suitable for a large area of applications (e.g., sensors, antireflective coatings, or photodetectors). For instance, while 1% Ca:ZnO at 0.5 M presents the highest porosity

(e.g., 23%), 5% Ca:ZnO at 0.5 M shows the lowest resistivity (e.g., 4.7 Ω cm).

2 Experimental details

2.1 Materials

All reagents, zinc acetate dihydrate ($Zn(CH_3COO)_2·2H_2O$, 99%), absolute ethanol (C_2H_6O, ≥99.8%), monoethanolamine (C_2H_7NO, MEA, ≥99%) were of analytical grade and were purchased from Sigma-Aldrich. Calcium chloride ($CaCl_2$, ≥93%) was used as the doping source. Microscope slides (Carl Roth), were used as substrates for optical analysis, SiO_2/Si substrates—Si (100), n-type, 1–10 Ω cm (300 nm thickness) were used for SEM, AFM, XRD, and electrical analysis and Si (100) substrates - p-type, 10–20 Ω cm were used for FTIR analysis.

2.2 Calcium doped ZnO synthesis

Nanostructured undoped ZnO thin film and Calcium ions doped ZnO thin films with 1 and 5% dopant concentration have been deposited using sol–gel spin-coating method on glass, Si, and Si/SiO_2 substrates. Two set of films have been prepared, the first set contains 0.25 M and the second one contains 0.5 M concentration. Further, the ZnO, 1 at% Ca:ZnO and 5 at% Ca:ZnO thin films samples will be named: ZnO, 1-Ca:ZnO, and 5-Ca:ZnO. The molar ratio of MEA to zinc acetate was 1.0 and the concentration of zinc acetate was 0.25 and 0.5 M. All solutions were prepared for 2 h at a temperature of 60 °C and the thin films were deposited on the substrate by spin coating at 3000 rpm during 30 s. The drying process was carried out, after each deposition, at temperature of 300 °C for 60 s in order to evaporate any remaining solvent and organic compound. Deposition fallowed by drying process was repeated for five times. Finally, the deposited layers were annealed to enhance their stability, at 500 °C for 1 h in the air atmosphere.

### 2.3 Characterization of the thin films

Chemical bonds configurations study of obtained films was carried out by Fourier Transform Infrared spectroscopy (FTIR) using Bruker Optics Vertex 80V Spectrometer, equipped with a transmission accessory unit. IR spectra were recorded after 64 scans with a 4 cm^{-1} resolution, in a spectral range of 4000–400 cm^{-1}. All spectra have been processed, the bands that can be attributed to the vibration mode of the C=O bonds of CO_2 were extracted. Surface morphology and the film thickness were evaluated by FEI Nova NanoSEM 630 Scanning Electron Microscope (FEG-SEM) using a ultra-high resolution detector at an acceleration voltage of 10 kV. The identification of Ca concentration and its distribution within the ZnO films were performed with the Element energy dispersive spectroscopy (EDS) system (Smart Insight AMETEK). The Energy dispersive X-ray spectroscopy (EDX) map was acquired at an acceleration voltage of 10 kV, with a working distance of 5 mm and ×30k magnification. EDX mapping have been used to assess the nanoscale composition and local distribution of elements in the polycrystalline films. The surface topography and roughness of films have been investigated using an atomic force microscope, AFM NTEGRA Aura - NT-MDT. The AFM measurements were performed in ambient atmosphere using a standard silicon cantilever in intermittent contact mode. The roughness parameter (RMS) of the surface were calculated on a 1 × 1 μm scanning area. XRD measurements were carried out on a Rigaku SmartLab X Ray Diffractometer using CuKα radiation ($λ = 1.5406$ Å) in Grazing Inccident (GI-XRD) mode with a incident angle of 0.5°. It was used a sampling step of 0.01° and a speed of 4°/min. The phase identification was made by referring to the International Center for Diffraction Data—ICDD database. The Micro-Raman spectra were recorded by a high-resolution Micro-Raman spectrometer LabRAM HR 800, HORIBA Jobin Yvon at excitation wavelength of 632.8 nm in the 200–600 nm spectral domain. The optical transmission and absorption properties of the films were measured with a HITACHI U-0080 D spectrophotometer, in the spectral range of 300–1100 nm. The thickness and refractive index (n) of the obtained films were determined by using Spectral Ellipsometer (SE 800 XUV) SENTECH. The electrical characteristics of the films were measured using a 4200-SCS/C/Keithley system coupled with an EP6/Suss MicroTec microprober, in dark and under light conditions. For this purpose, Ti/Au (10/100 nm) contacts with channel width/length (W/L) of 2000 μm/ 250 μm were fabricated by DC Sputtering on the films surface.

3 Results and discussions

Figure 1 shows the FTIR spectra of undoped (ZnO) and Ca-doped ZnO thin films (1-Ca:ZnO and 5-Ca:ZnO) with 1 and 5% dopant concentration at two different 0.25 and 0.5 M concentrations, respectively. The spectra exhibit only the bands in the range below 1200 cm^{-1}, characteristic to Si–Si, Si–O, and Zn–O vibrations of substrate and film structure. Thus, the peaks appearing in the spectral region between 450 and 400 cm^{-1} could be assigned to Si–O bonds from substrate or Zn–O from the thin films. In the case of thin film samples, the band shape suggests the Zn–O vibrational mode, but for a clearer understanding, the substrate contribution was subtracted. Possible assignments for the obtained peaks are presented in Table 1.

Fig. 1 Initial FTIR spectra **a** and after substrate subtraction **b** for undoped and Ca-doped ZnO thin films at 0.25 and 0.5 M concentration
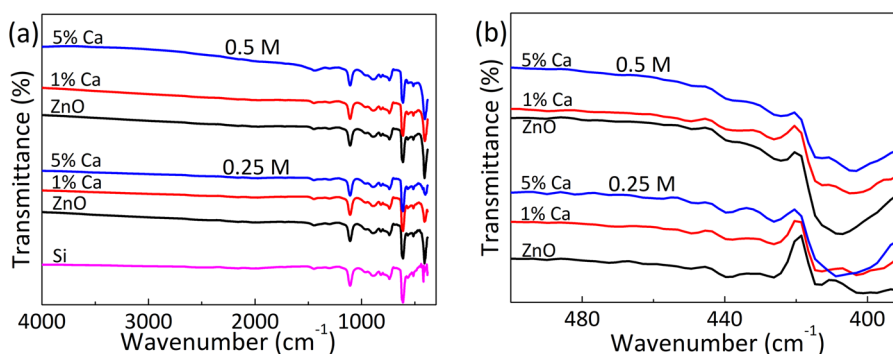
Table 1 The possible assignments for undoped and Ca-doped ZnO thin films at 0.25 and 0.5 M sol concentration, after substrate subtraction

Probable assignment	0.25 M			0.5 M		
	ZnO	1-Ca:ZnO	5-Ca:ZnO	ZnO	1-Ca:ZnO	5-Ca:ZnO
Si–O–Si	928	927	926	–	–	916
Zn–O	426	426	426	424	426	424
Zn–O	414	414	–	–	–	414
Zn–O	–	403	408	408	404	404

For 0.25 M concentration, the band shape obtained is related to metal oxide bonds and can be attributed to the vibrational assignment of Zn–O bond [22]. In the case of 0.5 M concentration, the spectra of ZnO and 1-Ca:ZnO films are defined only by absorption bands from 430–400 cm^{-1} spectral domain, suggesting a complete process was achieved based on to the presence of Zn–O bonds. Moreover, the 5-Ca:ZnO spectrum in 430–400 cm^{-1} domain displays the peaks assigned to the formation of Zn–O bonds. For all doped films the presence of dopant cannot be detected due to the fact that Ca–O bond overlaps with the Zn–O spectral bands in that particular region. However, in the case of the doped films at 0.5 M concentration a slight shift to lower wavenumbers was observed due to the difference between bond lengths when Ca^{2+} ion replaces Zn^{2+} ion.

The surface morphology and the thickness of ZnO, 1-Ca:ZnO, and 5-Ca:ZnO thin films in the case of 0.25 and 0.5 M concentration are shown in Fig. 2.

SEM analysis reveals randomly distributed spherical nanograins with different sizes separated by voids. The thin films are constructed of closely packed porous structures of ZnO nanograins.

In order to calculate mean nanograin size (s) and the surface porosity (P_S) in SEM images (presented in Table 3) we used open-source ImageJ analysis software where for the P_S we estimated the area covered by voids and nanograins on each image. Consequently, the surface porosity

increases with the rise of Ca dopant, except the case with 5-Ca:ZnO at 0.5 M concentration where the porosity decreases, because this film is more compact in which smaller grains are more effectively packed, giving denser structure. Regarding the calculated mean nanograin size, it is clearly observed that at 0.25 M concentration, the mean nanograin size increases with rise of Ca concentration (from 17 to 58 nm), but there 0.5 M, a contradictory trend can be observed (27–32 nm except for 5-Ca:ZnO film with 20 nm). Since the increase of the surface porosity is related to the possibility of sensitivity improvement [23], this type of spherical porous morphology becomes suitable for gas sensing applications.

From the cross-sectional images presented in the inset of the micrographs, we measured the film thickness. Thereby, we observed that the films thickness increases with about 14 nm towards to dopant concentration ($h_{1-Ca:ZnO} = 162$ nm and $h_{5-Ca:ZnO} = 176$ nm) in the case of 0.25 M. A similar trend can be observed in the case of 0.5 M when the thickness increases with about 207 nm ($h_{1-Ca:ZnO} = 239$ nm and $h_{5-Ca:ZnO} = 446$ nm). Also, the thickness of undoped ZnO film increased from 212 to 271 nm as a function of molarity concentration. We consider that the undoped films are thicker in comparison with the doped ones due to the existence of doping atoms in ZnO which modify the relative energy of the crystal faces according to Ganbavle et al. [24]. Furthermore, the substitution of doping atoms for Zn sites decreases the nucleation sites on the surface of substrate according to Nimbalkar et al. [25].

The % Ca content for 5-Ca:ZnO film (0.5 M) determined by EDX analysis shown in Fig. 3c, is 2.6% which is in good agreement with the Ca concentration which mixed in the sol. The Ca, O, Zn, and Cl elemental maps shown in Fig. 3b have the same spatial distribution which indicates a uniform distribution of elements in the synthesized films and demonstrates that the ZnO films are homogenously doped with Ca. As shown in Fig. 3b, Ca, O, Zn were the dominated elements in the deposited layers. However, the presence of other elements such as chloride ions is due to the prior contaminations with calcium chloride which was used as the doping source.

Fig. 2 Surface morphology (inset: cross-sectional image) of undoped and Ca-doped ZnO thin films: ZnO **a**, 1-Ca:ZnO **b** 5-Ca:ZnO **c** at 0.25 M and ZnO **d**, 1-Ca:ZnO **e** and 5-Ca:ZnO **f** at 0.5 M
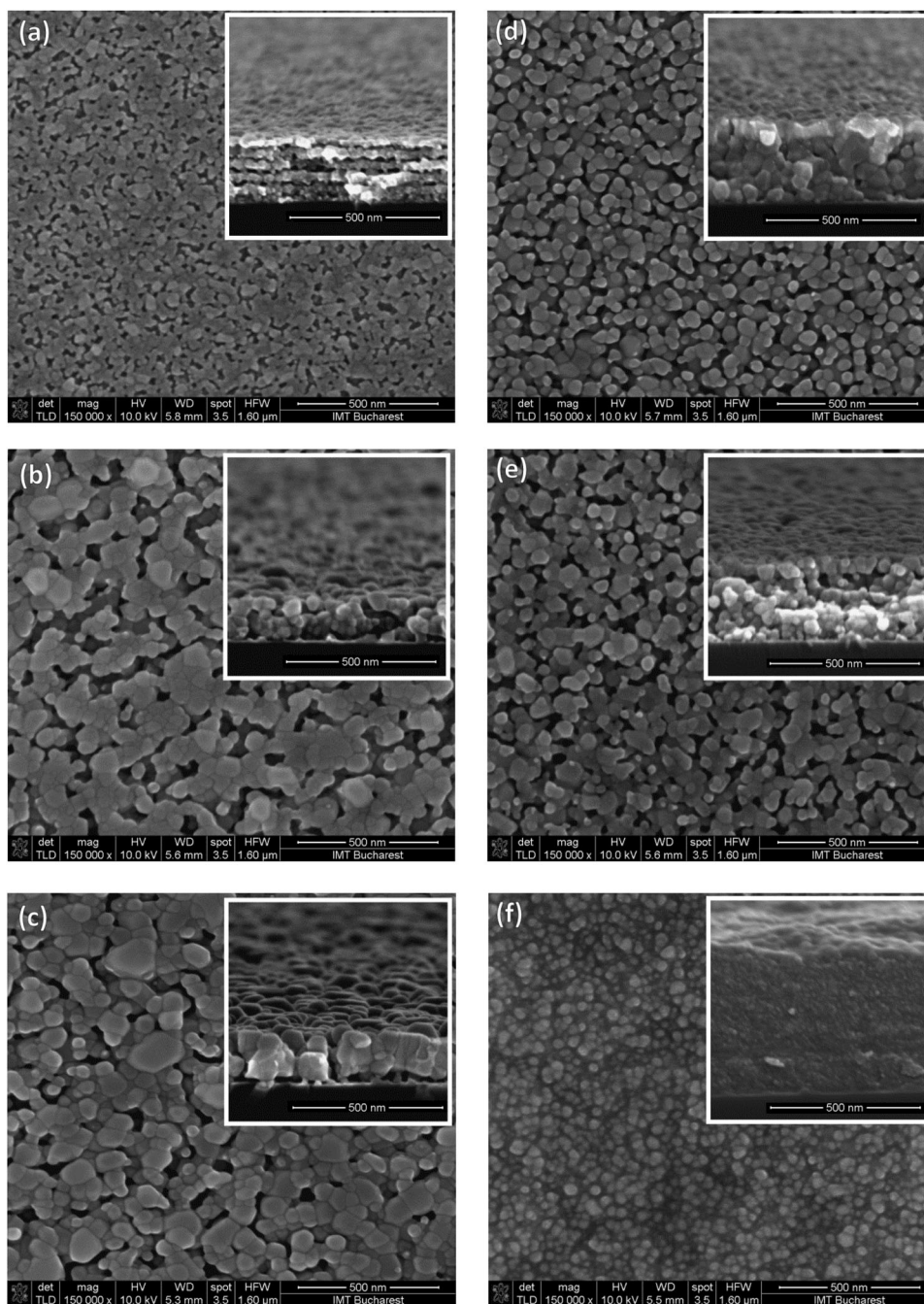
The AFM images of undoped and Ca-doped ZnO thin films, at 0.25 and at 0.5 M concentration are presented in Fig. 4. Furthermore, the surface roughness (RMS) of obtained films was calculated.

AFM images proves that the surface morphologies of the ZnO films are strongly dependent on the dopant concentration. The surface roughness (RMS) of ZnO film (6.9 nm) decreases with Ca doping reaching 5.1 nm for 1 at% Ca and 6.4 nm for 5 at% Ca at 0.25 M concentration. Figure 4d–f shows that films corresponding to 0.5 M have different nanoscale grain sizes that caused them to exhibit higher

RMS roughness when compared with 0.25 M concentration. Hence, at 0.5 M concentration the surface roughness of ZnO film (11.3 nm) significantly increases when the film is doped with 1 at% Ca (30.3 nm) and decreases when the dopant concentration increases at 5 at% (11.7 nm).

From XRD analysis, see Fig. 5, it can be observed that the both undoped ZnO films reveal a wurtzite-type structure, with the diffraction peaks corresponding to ZnO zincite (JCPDS card no. 36-1451).

The X-ray diffraction analysis revealed that the nature and concentration of Ca^{2+}, the metal ions substituted,

Fig. 3 SEM micrograph **a**, EDX mapping pattern of the element distribution: Ca, O, Zn, and Cl **b** and the quantitative analysis spectra **c** of the 5-Ca:ZnO thin film at 0.5 M concentration
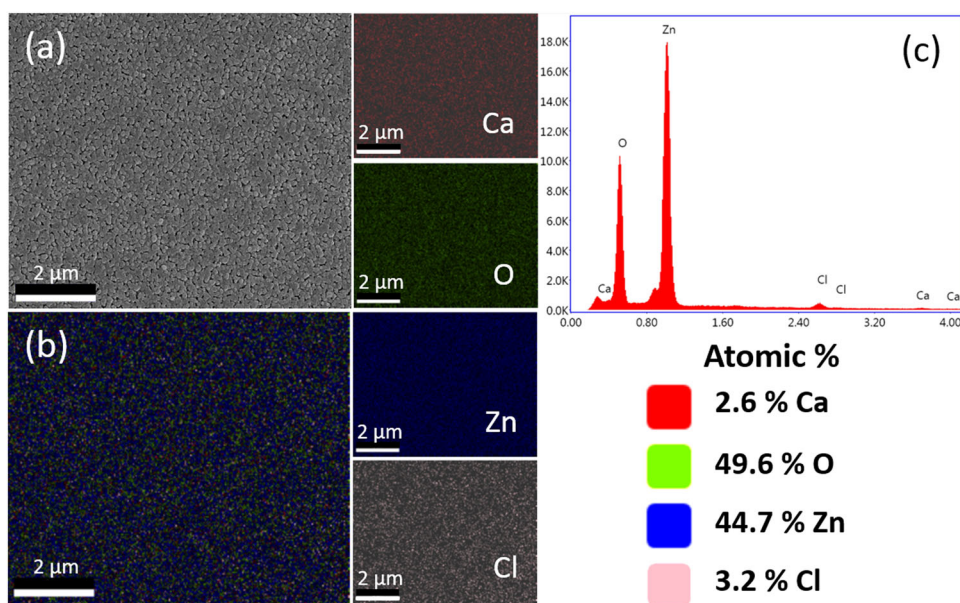
influence the formation of the crystal structure of ZnO lattice. With increasing the concentration of Ca, it can be noted on the one hand a broadening of the diffraction peaks, from 0.51° to 2.8° (5% Ca) and from 0.51° to 0.77° (5% Ca) for 0.25 and 0.5 M, respectively. On the other hand, a shift towards to smaller angles was observed suggesting the substitution of Zn^{2+} ions with Ca^{2+} inside the lattice was successful. Furthermore, it is important to remark that the all investigated samples exhibit preferential orientation on (002) atomic plane. This fact clearly indicates that the hexagonal wurtzite symmetry is preserved with Ca concentration. However, we noted an interesting behavior when ZnO lattice is doped with Ca. At 0.25 M, Ca leads to a decrease of (002) peak (i.e., from about 3600 cps to 620 cps). On the contrary, at 0.5 M, Ca leads to the increase of (002) peak intensity from 3000 to 3800 cps). We consider that the c-axis orientation (e.g., 002) in films when the concentration of Ca is greater is due to a self-texturing mechanism as discussed by Deng et al. [26] and Xu et al. [27] which implies minimization of surface energy and internal stress [28]. They concluded that the film crystal orientation is a result of a self-ordering effect caused by the minimization of the crystal surface free energy as well as by the interaction between the deposited material and the substrate surface. Also, the c-orientation might be resulted from the facilitated growth of the film along the c-axis as a result of the highest atomic density found along the (200) plane [29, 30]. Since the (002) and (103) diffraction peaks display the highest intensities, we focused our attention on these reflections. The dashed green and violet lines stand to ilustrate the angular position of (002) and (103) reflections, respectively of the undoped ZnO. It is known that when Ca^{2+} with a larger ionic radius (1.00 Å) substitutes Zn^{2+}

(0.74 Å) inside the ZnO wide lattice causes a shift of the reflections to smaller angles, which is commonly ascribed with the increasing of the lattice constant [18]. The lattice constants 'a' and 'c' for the investigated samples were derived from (103) and (002) reflections, respectively and are summarized in Table 2. Also, (103) diffraction peak exhibits a broadening from 0.77° to 1.52° (5% Ca) and from 0.51° to 1.01° (5% Ca) for 0.25 and 0.5 M, respectively. The peak broadening was evaluted using Full Width at Half Maximum (FWHM) value. It is important to remark that no supplementary phases compounds associated with Zn or Ca were detected, leading to the conclusion that the dopant does not change the wurtzite-type structure of ZnO. Also, the compactness high degree of the crystalline structure is indicated by the bond length between zinc and the oxygen ions, $L_{Zn–O}$ in the wurtzite type structure (see Table 2). These values are in good agreement with the standard 1.977 Å bond length of ZnO [31].

In order to estimate the mean crystallite size and the lattice strain was employed Whole-Powder-Pattern Fitting. The obtained results indicate a decreasing of the mean crystallite size decreases from 16 nm (ZnO) to 14 nm (1-Ca:ZnO) and then 3 nm (5-Ca:ZnO). This behavior was also observed for 0.5 M, where a decreasing from 25 nm (ZnO) to 22 nm (1-Ca:ZnO) and 12 nm (5-Ca:ZnO) was observed. In this context, ZnO thin films Ca-doped at the highest concentration (5% Ca) obtained at 0.5 M exhibit a better quality.

In order to estimate the mean crystallite size and the lattice strain was employed Whole-Powder-Pattern Fitting. The obtained results indicate a decreasing of the mean crystallite size decreases from 16 nm (ZnO) to 14 nm (1-Ca:ZnO) and then 3 nm (5-Ca:ZnO). This behavior was also

Fig. 4 AFM images of $1 \times 1\,\mu m$ scanned areas of undoped and Ca-doped ZnO thin films: ZnO **a**, 1-Ca:ZnO **b** and 5-Ca:ZnO **c** at 0.25 M and ZnO **d**, 1-Ca:ZnO **e** and 5-Ca:ZnO **f** at 0.5 M
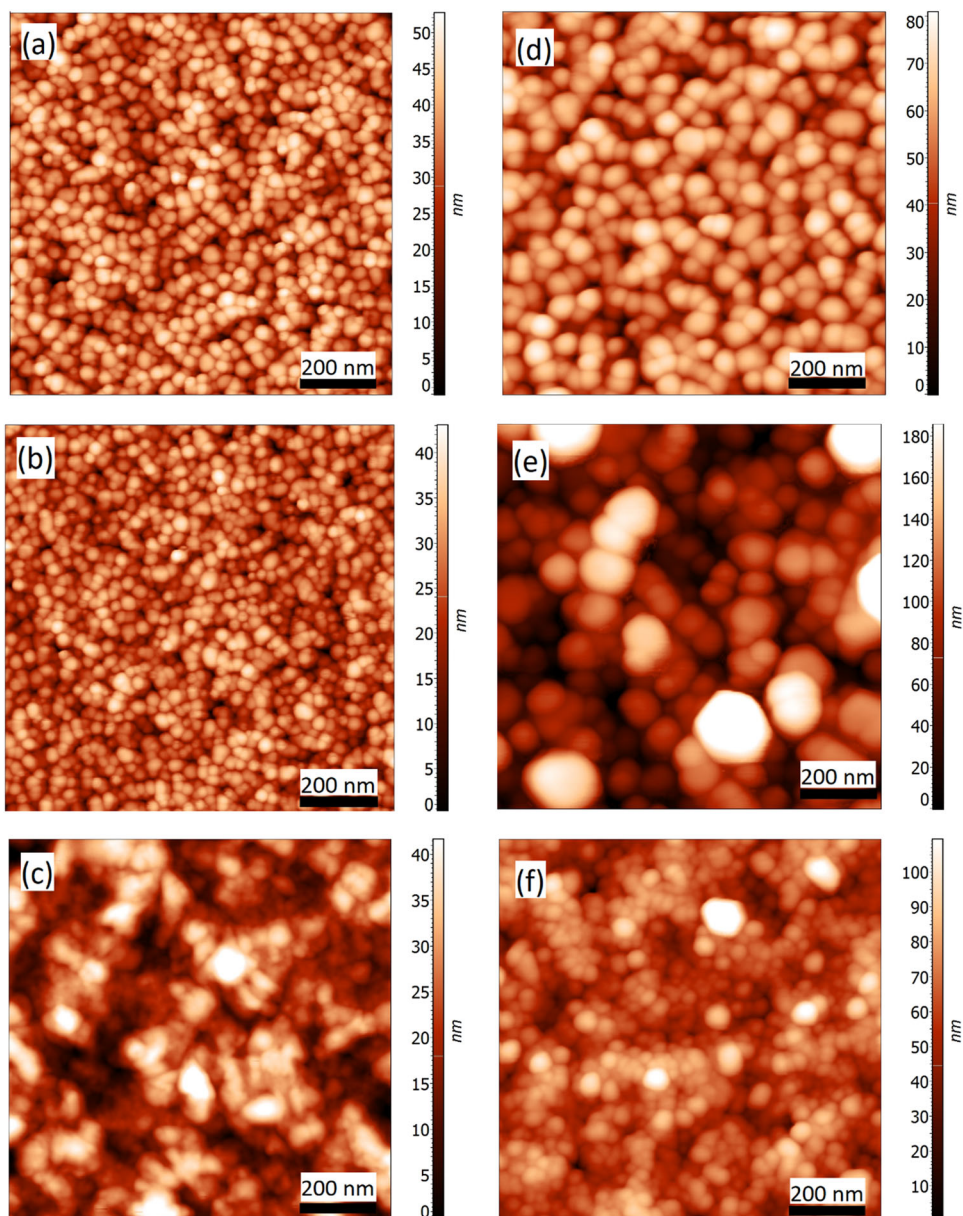
observed for 0.5 M, where a decreasing from 25 nm (ZnO) to 22 nm (1-Ca:ZnO) and 12 nm (5-Ca:ZnO) was observed. In this context, ZnO thin films Ca-doped at the highest concentration (5% Ca) obtained at 0.5 M exhibit a better quality.

The positions of the (103) and (002) diffraction peaks, the lattice constants a and c evaluated with the Bragg relation, the average crystallite size D_R, the lattice strain ε_R (estimated from Whole-Powder-Pattern Fitting) and the Zn─O bond length (L) calculated from the experimental XRD data [32] are presented in Table 2.

The Raman spectra of undoped and Ca-doped ZnO thin films, at 0.25 and at 0.5 M are presented in Fig. 6.

Wurtzite structure ZnO belongs to space group C6 and, according to group theory, the corresponding zone-center optical phonons are A1 + 2B1 + E1 + 2E2. The A1, E1, 2E2 modes are Raman active while 2B1 are silent. The polar phonons of A1 and E1 modes are split into longitudinal optical (LO) and transversal optical (TO) components: A1 (TO), A1 (LO), E1 (TO), E1 (LO) [33]. Generally, the E2 (high) and E2 (low) are the high and low wave number modes associated with the motion of oxygen atoms (O) and zinc (Zn) sublattices [34]. The high frequency E2 mode, the E2 (high) involves predominantly the lighter oxygen atoms and ZnO wurtzite structure [35, 36], while E2 (low) mode is associated with the nonpolar vibration of heavier cations Zn sublattice [37].

The Raman spectra of all the thin films exhibit the E2 (high) mode at ~439 cm^{-1} associated with bulk ZnO [38, 39]. The strong E2 (high) mode indicates there is a

Fig. 5 X-ray diffraction patterns of undoped and Ca-doped ZnO thin films: 0.25 M **a** and 0.5 M **b**. The dashed green and violet lines were used to show the position of the (002) and (103) reflections, respectively
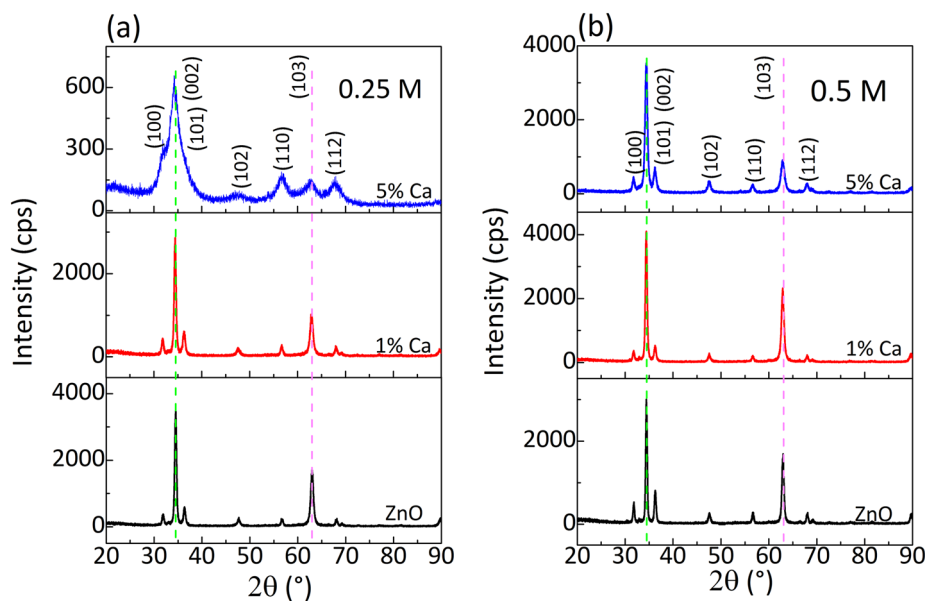
Table 2 The position of the (002) diffraction peak, the lattice constants a and c evaluated with the Bragg relation, the average crystallite size D_R and the lattice strain ε_R (Rieveld analysis) and the Zn—O bond length (L) for undoped and Ca-doped ZnO thin films at 0.25 and 0.5 M concentration

Film	(103) [°]	(002) [°]	a [Å]	c [Å]	D_R [nm]	ε_R [%]	L [Å]
0.25 M							
ZnO	62.92	34.50	3.275 ± 0.05	5.19 ± 0.14	16	0.12	1.974
1-Ca:ZnO	62.86	34.42	3.277 ± 0.05	5.210 ± 0.14	14	0.03	1.976
5-Ca:ZnO	62.82	34.21	3.284 ± 0.05	5.230 ± 0.14	3	0.42	1.969
0.5 M							
ZnO	62.92	34.44	3.275 ± 0.05	5.203 ± 0.14	25	0.26	1.976
1-Ca:ZnO	62.82	34.41	3.277 ± 0.05	5.206 ± 0.14	22	0.38	1.977
5-Ca:ZnO	62.80	34.40	3.288 ± 0.05	5.207 ± 0.14	12	0.23	1.977

The associated errors were estimated taking into account the used optical instruments (i.e., without monochromator at the incidence and PSA 0.5° at detector)

good crystallinity in both the undoped and the Ca doped ZnO films. The Raman spectra of the Ca-doped ZnO thin films does not show any additional modes indicating the achievement of a high-quality thin films. Also, Raman spectroscopy results are in good agreement with XRD results and confirm the hexagonal phase of thin films.

The optical transmission and absorption spectra of the films are displayed in Fig. 7.

The films transmittance spectra indicate values of 81–93%, except for 5-Ca:ZnO film (0.25 M) in which case the transmittance in the (350–800 nm) wavelength region decreases significantly (73%). Higher transmittance obtained for 5-Ca:ZnO film (0.5 M) may emerge from the structural homogeneity and crystallinity of 5-Ca:ZnO film as evidenced from AFM and XRD analysis. The optical band gaps ($E_{g,optic}$) were estimated from the absorption edge

using the Tauc relation and further extrapolation of the linear region of $(\alpha h\nu)^2$ versus $h\nu$ plot [40]. We remarked at both 0.25 and 0.5 M concentration that the band gap decreases with increasing dopant concentration which could be associated to the merging of an impurity band into the conduction band thereby shrinking the band gap [41, 42]. Formation of such impurity band give rise to new donor electronic states just below the conduction band due to hybridization between states of the ZnO matrix and that of the dopants [41, 42]. Consequently, the band-gap values reported in our study ~3.22 eV are slightly smaller than the bulk value of 3.3 eV according to Islam et al. [43] and is in good agreement with previously reported results that also showed the decrease in the band gap of Ca doped ZnO nanoparticles [44], Ca doped ZnO nanorods [45], ZnO thin films [46], and Al doped ZnO thin films [47]. This slight
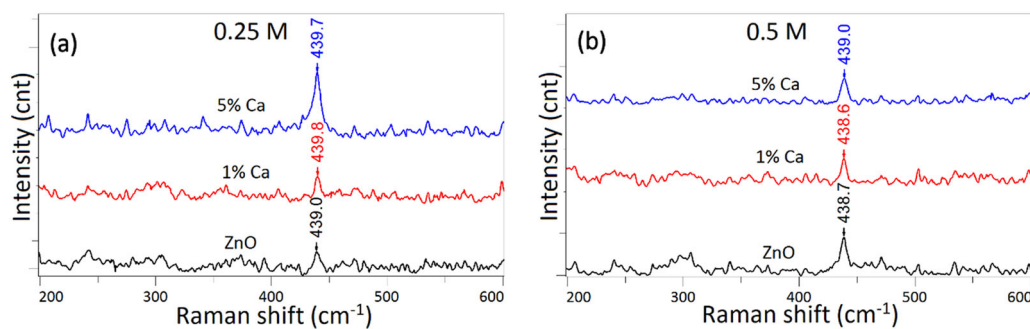
Fig. 6 Micro-Raman spectra of undoped and Ca-doped ZnO thin films at 0.25 M and at 0.5 M

Fig. 7 Transmission spectra of undoped and Ca-doped ZnO thin films: at 0.25 M **a** and at 0.5 M **b**. Inset: absorption spectra of the films
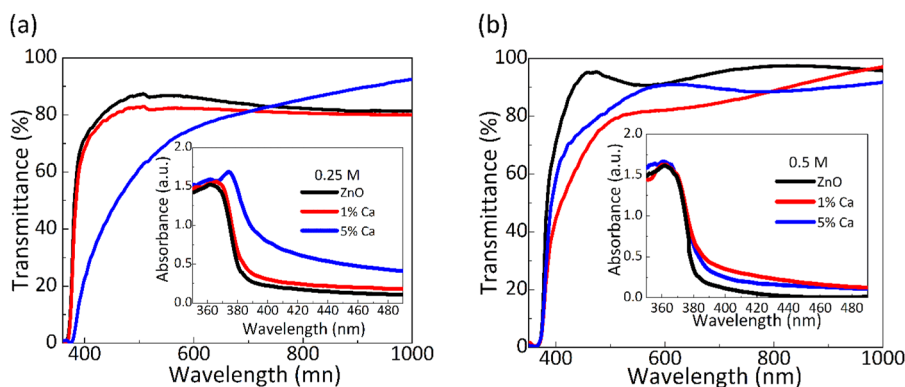
Table 3 Refractive index (n), volume porosity (P_V), surface porosity (P_S), mean nanograin size (s) transmission (T), optical band gap ($E_{g,optic}$) and resistivity (ρ) for undoped and Ca-doped ZnO thin films at 0.25 M and at 0.5 M concentration

| Film	n	P_V (%)	P_S (%)	s (nm)	T (%)	$E_{g,optic}$ (eV)	ρ (Ω cm)
0.25 M							
ZnO	1.84	11	13	17	84	3.23	88.02
1-Ca:ZnO	1.73	20	24	39	81	3.22	26.69
5-Ca:ZnO	1.75	18	17	58	73	3.10	23.51
0.5 M							
ZnO	1.96	2	6	27	93	3.24	22.33
1-Ca:ZnO	1.70	23	32	32	84	3.21	1391.93
5-Ca:ZnO	1.90	7	12	20	90	3.22	4.70

difference is due to the fact that the values of E_g depend on many factors e.g., the granular structure, the nature and concentration of precursors, the structural defects, and the crystal structure of the films [48]. Furthermore, the grain boundary, the stress and the interaction potentials between defects and host materials in the films influenced the properties of ZnO films. The values of transmission (T) and the calculated optical band gap ($E_{g,optic}$) corresponding to all the prepared thin films are listed in Table 3. It is notable that 5-Ca:ZnO film (0.25 M) exhibits a reduced $E_{g,optic}$, which suggests a presence of defects, nonstoichiometry, and crystal imperfection [49].

Optical constants of sol–gel deposited thin films have been investigated by Spectroscopic Ellipsometry. Layer

volume porosity decreases from thin film surface to bottom. We have used a model where the distribution of porosity in the ZnO layer is approximated by two layers having distinct porosities. The layer situated at the thin film surface has the highest porosity. According to the ellipsometry analysis, the refractive index (n) and porosity (P) corresponding to the less porous layer are also presented in Table 3.

Both ZnO and 5-Ca:ZnO films are denser compared with 1-Ca:ZnO at 0.5 M and at 0.25 M, as indicated by the values of the refractive index and volume porosity values. The volume porosity (P_V) of the films has been calculated using Lorentz–Lorentz equation [50]. To get an additional estimation of the surface porosity (S_V), we used top-view SEM images, taking into account the area covered by voids and

Fig. 8 Electrical characteristics (*I–V*) measured under dark and white light conditions: ZnO **a**, 1-Ca:ZnO **b** and 5-Ca:ZnO **c** at 0.25 M and ZnO **d**, 1-Ca:ZnO **e** and 5-Ca:ZnO **f** at 0.5 M
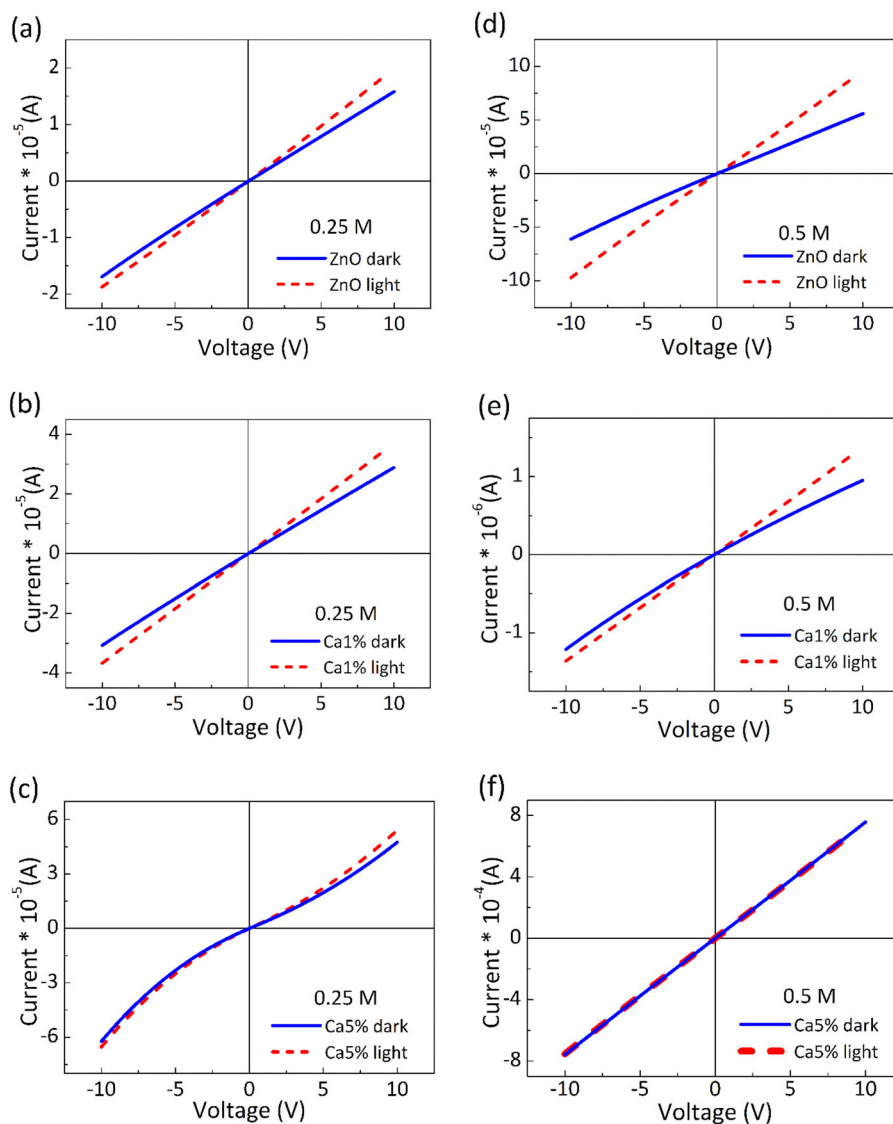
nanograins, respectively. Ca-doped ZnO films displayed higher volume porosity with respect to the undoped samples, confirming that an addition of Ca modifies the morphology and the grain size, in general agreement with the previously presented morphological analysis. It appears that adatoms increase the porosity at both 0.25 and 0.5 M concentration and consequently they influence also the refractive index. As a general trend, the lowest values of the refractive index (*n*) were determined to be 1.73 and 1.70 in case of 1-Ca:ZnO at 0.25 and at 0.5 M, respectively. Furthermore, the maximum porosity, was 20 and 23% obtained in the same case of 1-Ca:ZnO at 0.25 and 0.5 M, respectively. Following the ellipsometry analysis, it was found that the porosity is influenced by the molar concentration and by the amount of dopant. The refractive index increased from 1.75 (5-Ca:ZnO, 0.25 M) to 1.90 (5-Ca:ZnO, 0.5 M), due to increasement of films density as well as improved

crystallinity, as evidenced by X-ray diffraction (XRD) and Micro-Raman Spectroscopy.

I–V characteristics of the films fabricated using sol–gel spin coating technique measured under dark and white light conditions are plotted in Fig. 8. The electrical conductivity of ZnO thin films is dominated by charge generated from Zn interstitial atoms and oxygen vacancies [51]. Therefore, the decrease in resistivity of ZnO films by Ca doping may be due to zinc interstitials and/or oxygen vacancies in the films.

The prepared films present a low conductivity along with a small sensitivity under ambient light. One can be observe a resistive characteristic in ZnO at 0.25 M (see Fig. 8 (a)), conversely at 5-Ca:ZnO the *I–V* characteristic is slowly nonlinear. At 0.5 M, in the case of 5-Ca:ZnO thin film, it can be seen that electrical resistance decreased by one order of magnitude compared with the others films, possibly because the film morphology shows a reduced roughness

and porosity. Also, it is noticeable the improvement in terms of electrical resistance value compared with ZnO film obtained at the same concentration of 0.5 M, while the illumination does not influence the electrical behavior. In accordance with Dahoudi [52], we argue that intergranular voids and pores create discontinuities between nanograins, thus inhibiting the smooth mobility of charge carriers and resulting in a relatively high electrical resistivity as we have observed for 1% Ca, 0.5 M. Also, high resistivity for 1% Ca, 0.5 M can be interpreted as the calcium oxide related precipitates, which form at the grain boundaries that may act as scattering centers [53]. Therefore, in this study the appearance of very few pores and voids as revealed by SEM and AFM analyses, hence, less discontinuities between nanograins, gives rise to the obtained lowest electrical resistivity of 4.70 Ω cm (corresponding to 5% Ca, 0.5 M) which is lower than 28.2 Ω cm reported by Natsume et al. [54] and 21.1 Ω cm reported by Talukder et al. [55]. These results corroborate well with the ellipsometry analysis, where the 5-Ca:ZnO film, 0.5 M exhibit the lowest porosity (7%) and present a denser smoother structure, as we have observed in cross-sectional SEM image. The lowest resistivity obtained for 5-Ca:ZnO film (0.5 M) indicates the generation of additional carriers due to the contribution from Ca^{2+} ions on substitutional sites of Zn^{2+} ions. We believe that the denser structure, lower porosity and increased crystalline orientation are responsible for the significant improvement in resistivity of the deposited films. Also, it is known that the electrical resistivity of ZnO nanostructures gradually decreases with respect to the mean crystallite size, and nanostructure orientation [56]. We remarked that the 5-Ca:ZnO thin film at 0.5 M concentration exhibit superior properties, regarding the resistivity when compared with 0.25 M concentration. This fact is also confirmed by X-ray diffraction, when Ca doping has a different impact. More precisely, at 0.25 M, Ca leads to a decrease of (002) peak (i.e., from about 3600 cps to 620 cps). On the contrary, at 0.5 M, Ca leads to the increase of (002) peak intensity from 3000 to 3800 cps. The incorporation of Ca into ZnO improves the electrical conductivity due to the creation of one extra carrier as a result of substitutional doping of Ca^{2+} at Zn^{2+} sites [57]. In the present work, the higher dopant content (5-Ca:ZnO), at 0.5 M sol concentration gave the more intense peaks, which underlines the enhancement of the films crystallization. Therefore, this film presents the lowest resistivity.

4 Conclusions

To conclude, ZnO thin films with 0.25 and 0.5 M molarity concentration which consist of undoped and Ca doped ZnO with 1 and 5 at% were deposited by a facile sol–gel spin coating method on SiO_2/Si, Si, and glass substrate. FTIR spectra confirmed the presence of Zn–O bonds and a slight shift to lower wavenumbers, which could confirm the doping of the films due to the difference between bond lengths when Ca^{2+} ion replaces Zn^{2+} ion. The EDX mapping indicates that Ca is homogenously dopped in the ZnO films. EDX analysis confirms the presence of 2.6% atomic weight of Ca in the ZnO matrix doped with 5% Ca (0.5 M), which was uniformly distributed at the surface of the substrate. Surface morphology investigations clearly indicate an increasing of the surface porosity with Ca concentration. Also, XRD analysis reveals structural modifications with Ca concentration, in terms of both lattice parameters and crystallite sizes. Remarkable, the wurtzite structure of ZnO with (002) preferential orientation was preserved after the Ca incorporation. The wurtzite structure of ZnO was also evidencied by Raman spectroscopy. Regarding the optical properties were employed spectral ellipsometry and UV–Vis spectroscopy. On the one hand, spectral ellipsometry indicates a decreasing of the refractive index (from 1.70 to 1.96), accompanied with an increasing of the volume porosity (from 2 to 23%). On the other hand, UV–Vis spectroscopy indicates a decreasing of both transmitance (from 73 to 93%) and band gap value (from 3.10 to 3.24 eV). It is clear that the wide range of volume porosity for the investigated samples could constitute a starting point for sensors. Also, electrical measurements showed a modification of the resistivity with Ca doping.

Compliance with ethical standards

Conflict of interest The authors declare that they have no conflict of interest.

Publisher's note Springer Nature remains neutral with regard to jurisdictional claims in published maps and institutional affiliations.

References

1. Nimbalkar AR, Patil NB, Ganbavle VV, Mohite SV, Madhale KV, Patil MG (2019) Sol-gel derived aluminium doped zinc oxide thin films: a view of aluminium doping effect on physicochemical and NO_2 sensing properties. J Alloy Compd 775:466–473

2. Yu W, Han D, Cui G, Cong Y, Dong J, Zhang X, Zhang X, Wang Y, Zhang S (2016) High-performance calcium-doped zinc oxide thin-film transistors fabricated on glass at low temperature. Jpn J Appl Phys 55:1–4

3. Yu W, Han D, Shi P, Cong Y, Zhang Y, Dong J, Zhou X, Huang L, Cui G, Zhang S, Zhang X, Wang Y (2015) Effects of substrate temperature on performance of calcium-doped zinc oxide TFTs. Electron Lett 51:1286–1288

4. Wong LLP, Na S, Chen AI, Li Z, Macecek M, Yeow JTW (2016) A feasibility study of piezoelectric micromachined ultrasonic transducers fabrication using a multi-user MEMS process. Sens Actuat A—Phys 247:430–439

5. Bhatia D, Sharma H, Meena RS, Palkar VR (2016) A novel ZnO piezoelectric microcantilever energy scavenger: Fabrication and characterization. Sens Biosensing Res 9:45–52

6. A Ghosh, C Zhang, S Shi, H Zhang (2019) High temperature CO_2 sensing and its cross-sensitivity towards H_2 and CO gas using calcium doped ZnO thin film coated langasite SAW sensor. Sensor Actuat. B-Chem https://doi.org/10.1016/j.snb.2019.126958

7. Salim ZT, Hashim U, Md. Arshad MK, Fakhri MA, Salim ET (2017) Zinc oxide flakes-corolla lobes like nano combined structure for SAW applications. Mater Res Bull 86:215–219

8. Nazir Kayani Z, Sahar S, Riaz S, Naseem S (2019) Tuning of optical and antibacterial characteristics of ZnO thin films: role of Ce content. Ceram Int 45:3930–3939

9. Water W, Wang S-F, Chen Y-P, Pu J-C (2005) Calcium and strontium doped ZnO films for love wave sensor applications. Integr Ferroelectr 72:13–22

10. Dhahri R, Hjiri M, El Mir L, Fazio E, Neri F, Barreca F, Donato N, Bonavita A, Leonardi SG, Neri G (2015) ZnO:Ca nanopowders with enhanced CO_2 sensing properties. J Phys D: Appl Phys 48:1–7

11. Hjiri M, Zahmouli N, Dhahri R, Leonardi SG, El Mir L, Neri G (2017) Doped-ZnO nanoparticles for selective gas sensors. J Mater Sci: Mater Electron 28:9667–9674

12. Dhahri R, Leonardi SG, Hjiri M, El Mir L, Bonavita A, Donato N, Iannazzo D, Neri G (2017) Enhanced performance of novel calcium/aluminum co-doped zinc oxide for CO_2 sensors. Sens Actuators B 239:36–44

13. Mahdhi H, Djessas K, Ben Ayadi Z (2018) Synthesis and characteristics of Ca-doped ZnO thin films by rf magnetron sputtering at low temperature. Mater Lett 214:10–14

14. Samuel EP, Bhadane H, Chandra U, Gautam DK (2014) Sol gel Spin coated ZnO thin films for biosensing applications. Int J Eng Technol Res 2:42–44

15. Znaidi L (2010) Sol–gel-deposited ZnO thin films: a review. Mater Sci Eng B 174:18–30

16. Ammaih Y, Lfakir A, Hartiti B, Ridah A, Thevenin P, Siadat M (2014) Structural, optical and electrical properties of ZnO:Al thin films for optoelectronic applications. Opt Quant Electron 46:229–234

17. Water W, Yang Y-S (2006) The influence of calcium doped ZnO films on Love wave sensor characteristics. Sens Actuators A 127:360–365

18. Cao L, Jiang J, Zhu L (2013) Realization of band-gap engineering of ZnO thin films via Ca alloying. Mater Lett 100:201–203

19. Santangelo S, Patanè S, Frontera P, Pantò F, Triolo C, Stelitano S, Antonucci P (2017) Effect of calcium- and/or aluminum-incorporation on morphological, structural and photoluminescence properties of electro-spun zinc oxide fibers. Mater Res Bull 92:9–18

20. Ghiloufi I, El Ghoul J, Modwi A, El Mir L (2016) Preparation and characterization of Ca-doped zinc oxide nanoparticles for heavy metal removal from aqueous solution. MRS Adv 1:3607–3612

21. Karthikeyan B, Pandiyarajan T, Mangaiyarkarasi K (2011) Optical properties of sol–gel synthesized calcium doped ZnO nanostructures. Spectrochim Acta A: Mol Biomol Spectrosc 82:97–101

22. Ivanova T, Harizanova A, Koutzarova T, Vertruyen B (2010) Study of ZnO sol–gel films: effect of annealing. Mater Lett 64:1147–1149

23. Nimbalkar AR, Patil MG (2017) Synthesis of ZnO thin film by sol-gel spin coating technique for H_2S gas sensing application. Physica B 527:7–15

24. Ganbavle VV, Patil SK, Inamdar SI, Shinde SS, Rajpure KY (2014) Effect of Co doping on structural, morphological and LPG sensing properties of nanocrystalline ZnO thin films. Sens Actuators A 216:328–334

25. Nimbalkar AR, Patil MG (2017) Synthesis of highly selective and sensitive Cu-doped ZnO thin film sensor for detection of H_2S gas. Mater Sci Semicond Process 71:332–341

26. Deng H, Russell JJ, Lamb RN, Jiang B, Li Y, Zhou XY (2004) Microstructure control of ZnO thin films prepared by single source chemical vapor deposition. Thin Solid Films 458:43–46

27. Xu Z, Deng H, Li Y, Guo QH (2006) Characteristics of Al-doped c-axis orientation ZnO thin films prepared by the sol–gel method. Mater Res Bull 41:354–358

28. Bao D, Gu H, Kuang A (1998) Sol-gel-derived c-axis oriented ZnO thin films. Thin Solid Films 312:37–39

29. Amirhaghi S, Craciun V, Craciun D, Elders J, Boyd IW (1994) Low temperature growth of highly transparent c-axis oriented ZnO thin films by pulsed laser deposition. Microelectron Eng 25:321–324

30. Raoufi D, Raoufi T (2009) The effect of heat treatment on the physical properties of sol-gel derived ZnO thin films. Appl Surf Sci 255:5812–5817

31. Ravichandran C, Srinivasan G, Lennon C, Sivananthan S, Kumar J (2011) Influence of post-deposition annealing on the structural, optical and electrical properties of Li and Mg co-doped ZnO thin films deposited by sol–gel technique. Superlattice Microstruct 49:527–536

32. Shaban M, El Sayed AM (2016) Effects of lanthanum and sodium on the structural, optical and hydrophilic properties of sol–gel derived ZnO films: a comparative study. Mater Sci Semicond Process 41:323–334

33. Musat V, Fortunato E, Purica M, Mazilu M, Botelho do Rego AM, Diaconu B, Busani T (2012) Multifunctional zinc oxide nanostructures for a new generation of devices. Mater Chem Phys 132:339–346

34. Kalyanaraman S, Vettumperumal R (2013) Study of multiple phonon behavior in Li-doped ZnO thin films fabricated using the sol-gel spin-coating technique. J Korean Phys Soc 62:804–808

35. Chai GY, Chow L, Lupan O, Rusu E, Stratan GI, Heinrich H, Ursaki VV, Tiginyanu IM (2011) Fabrication and characterization of an individual ZnO microwire-based UV photodetector. Solid State Sci 13:1205–1210

36. Vettumperumal R, Kalyanaraman S, Santoshkumar B, Thangavel R (2016) Estimation of electron–phonon coupling and Urbach energy in group-I elements doped ZnO nanoparticles and thin films by sol–gel method. Mater Res Bull 77:101–110

37. Chen LC, Tien C-H, Fu C-S (2012) Magneto-optical characteristics of Mn-doped ZnO films deposited by ultrasonic spray pyrolysis. Mater Sci Semicond Process 15:80–85

38. Orozco S, Riascos H, Duque S (2016) Raman spectroscopy of ZnMnO thin films grown by pulsed laser deposition. J Phys: Conf Ser 687:1–4

39. Ben Yahia S, Znaidi L, Kanaev A, Petitet JP (2008) Raman study of oriented ZnO thin films deposited by sol–gel method. Spectrochim Acta A 71:1234–1238

40. Bedia A, Bedia FZ, Aillerie M, Maloufi N, Benyoucef B (2015) Morphological and optical properties of ZnO thin films prepared by spray pyrolysis on glass substrates at various temperatures for integration in solar cell. Energy Proced 74:529–538

41. Girma T, Siraj K, Yifru A (2016) Defect induced band gap narrowing of zinc oxide nanoparticles using Li+, Na+ and K+ metal ions as a dopant. Elixir Mater Sci 91:38058–38062

42. Hasabeldaim E, Ntwaeaborwa OM, Kroon RE, Swart HC (2019) Structural, optical and photoluminescence properties of Eu doped ZnO thin films prepared by spin coating. J Mol Struct 1192:105–114

43. Islam MR, Podder J, Islam MM, Chowdhury RI, Farhad SFU, Saha DK (2011) Effect of annealing on the structural and optical properties of nano fiber ZnO films deposited by spray pyrolysis. Sens Transducers 134:170–176

44. Slama R, El Ghoul J, Omri K, Houas A, El Mir L, Launay F (2016) Effect of Ca-doping on microstructure and photocatalytic activity of ZnO nanoparticles synthesized by sol gel method. J Mater Sci: Mater Electron 27:7939–7946

45. Santoshkumar B, Kalyanaraman S, Vettumperumal R, Thangavel R, Kityk IV, Velumani S (2016) Structure-dependent anisotropy of the photoinduced optical nonlinearity in calcium doped ZnO nanorods grown by low cost hydrothermal method for photonic device applications. J Alloy Compd 658:435–439

46. Che Ani N, Kamaruddin SA, Nayan N, Tawil SNM, Sahdan MZ (2015) Effects of ageing time of ZnO sol on properties of ZnO films by sol gel spin coating. Int J Nanoelectron Mater 8:15–21

47. Aydın H, Yakuphanoglu F, Aydın C (2019) Al-doped ZnO as a multifunctional nanomaterial: structural, morphological, optical and low-temperature gas sensing properties. J Alloy Compd 773:802–811

48. Ahmed MAM, Meyer WE, Nel JM (2019) Structural, optical and electrical properties of the fabricated Schottky diodes based on ZnO, Ce and Sm doped ZnO films prepared via wet chemical technique. Mater Res Bull 115:12–18

49. Shakti N, Gupta PS (2010) Structural and optical properties of sol-gel prepared ZnO thin film. Appl Phys Res 2:19–28

50. Dutta M, Mridha S, Basak D (2008) Effect of sol concentration on the properties of ZnO thin films prepared by sol–gel technique. Appl Surf Sci 254:2743–2747

51. Bhat JS, Patil AS, Swami N, Mulimani BG, Gayathri BR, Deshpande NG, Kim GH, Seo MS, Lee YP (2010) Electron irradiation effects on electrical and optical properties of sol-gel prepared ZnO films J Appl Phys 108:043513-1–043513-8

52. Dahoudi NA (2014) Comparative study of highly dense aluminium and gallium doped zinc oxide transparent conducting sol–gel thin films. Bull Mater Sci 37:1243–1248

53. Mahdhi H, Ben Ayadi Z, Gauffier JL, Djessas K, Alaya S (2015) Effect of sputtering power on the electrical and optical properties of Ca-doped ZnO thin films sputtered from nanopowders compacted target. Opt Mater 45:97–103

54. Natsume Y, Sakata H (2000) Zinc oxide films prepared by sol–gel spin-coating. Thin Solid Films 372:30–36

55. Talukder A-A, Pokharel J, Shrestha M, Fan QH (2016) Improving electrical properties of sol-gel derived zinc oxide thin films by plasma treatment J Appl Phys 120:155303-1–155303-7

56. Davis K, Yarbrough R, Froeschle M, White J, Rathnayake H (2019) Band gap engineered zinc oxide nanostructures via a sol–gel synthesis of solvent driven shape-controlled crystal growth. RSC Adv 9:14638–14648

57. Nakrela A, Benramdane N, Bouzidi A, Kebbab Z, Medles M, Mathieu C (2016) Site location of Al-dopant in ZnO lattice by exploiting the structural and optical characterisation of ZnO:Al thin films. Results Phys 6:133–138